Regulation of endothelin-1 gene expression by cell shape and the microfilament network in vascular endothelium

ADEL MOUSSA MALEK,[1] IKE W. LEE,[3] SETH L. ALPER,[2] AND SEIGO IZUMO[3]
[1]*Department of Neurosurgery, Brigham and Women's Hospital, Children's Hospital, and Harvard Medical School, Boston, 02115; and* [3]*Cardiovascular Division and* [2]*Molecular Medicine and Renal Units, Beth Israel Deaconess Medical Center, and Departments of Medicine and Cell Biology, Harvard Medical School, Boston, Massachusetts 02215*

Malek, Adel Moussa, Ike W. Lee, Seth L. Alper, and Seigo Izumo. Regulation of endothelin-1 gene expression by cell shape and the microfilament network in vascular endothelium. *Am. J. Physiol.* 273 (*Cell Physiol.* 42): C1764–C1774, 1997.—Endothelial synthesis and release of endothelin-1 (ET-1) are exquisitely regulated by external shear and strain. We tested the hypothesis that manipulation of endothelial cell shape can regulate ET-1 gene expression. Treatment of bovine aortic endothelial cell (BAEC) monolayers with cytochalasin D disrupted F-actin and induced cell retraction and rounding, in parallel with time- and dose-dependent specific decreases in ET-1 mRNA levels. Treatments with forskolin, phorbol 12-myristate 13-acetate, staurosporine, and genistein also induced cell shape change and decreased F-actin staining and ET-1 mRNA levels. BAEC plated onto nonadhesive petri dishes coated with decreasing concentrations of synthetic RGD polymer showed RGD dose-dependent decreases in cell spreading and in F-actin microfilament elaboration. These changes were specifically accompanied by decreases in ET-1 peptide secretion (60%) and, via posttranscriptional mechanisms, ET-1 mRNA (94%) and were not due to decreased cell-cell contact. We conclude that the shape and microfilament network of endothelial cells are potent posttranscriptional regulators of ET-1 gene expression.

morphometry; mechanotransduction; gene expression; cytoskeleton; F-actin

THE ENDOTHELIAL CELL is continuously subjected to hemodynamic forces that elicit, in turn, structural and functional responses (6, 21). Numerous studies have documented that endothelial cell shape is determined by its external mechanical environment both in vivo (17, 27) and in vitro (29). When subjected to cyclic strain of the underlying extracellular matrix, endothelial cell monolayers undergo a transition in cell shape from polygonal to ellipsoidal and align along an axis perpendicular to the strain vector (33, 34). In response to flow, endothelial cell monolayers align in a parallel direction and assume a fusiform morphology in areas of high shear and a polygonal one in areas of low shear stress magnitude (11, 24). These differences in endothelial morphology in response to fluid shear stress are accompanied by changes in F-actin and microfilament cytoskeleton structure (9, 10, 14, 22).

In addition to the externally applied mechanical stimuli of shear and axial stress, endothelial cells have been shown to generate significant tension against the substratum (18, 26); this phenomenon has been observed by silicone-wrinkling techniques (13, 26) and quantified using direct isometric measurement (18). The contractile force generated by the endothelial cell is dependent on microfilament integrity and can be abolished by treatment with cytochalasin D (CytD) (18). Fluid shear stress applied in vitro also induces changes in the functional state of the endothelial cell, including an altered pattern of gene expression (6, 21) that is associated with chronic changes in the cytoskeleton and cell morphology (22). Shear stress induces, in addition, significant decreases in the rate of DNA synthesis (23) and in intracellular pH (38). These effects resemble those previously reported in endothelial cells grown in the round configuration (15, 16), with its associated decreased intracellular tension (1, 18). Furthermore, fluid shear stress induces downregulation of the vasoconstrictor endothelin-1 (ET-1) (20), a potent mitogen to vascular smooth muscle cells and cardiac myocytes (35), which has been proposed to play a central role in blood vessel homeostasis and structural remodeling (32). Taken together, these results suggest a link between external mechanical stimuli and endothelial gene expression that may be important in the long-term adaptation to the hemodynamic stimulus in vivo. Shear stress and mechanical strain also regulate the microfilament network and cell shape. Direct roles of the microfilament network and cell shape in control of gene expression remain poorly defined.

In this report, we investigate the link between the cell shape and microfilament network of endothelial cells and endothelial cell expression of the ET-1 gene. Our findings, obtained in a setting free of external mechanical stimulus, suggest that the status of microfilaments and cell shape themselves play an important role in the regulation of ET-1 production.

MATERIALS AND METHODS

Materials. All reagents used were of the highest available grade. CytD, phorbol 12-myristate 13-acetate (PMA), forskolin, genistein, and staurosporine were obtained from Sigma Chemical (St. Louis, MO) and ProNectin F from Protein Polymer Technologies (San Diego, CA).

Cell culture. Bovine aortic endothelial cells (BAEC; *passages 6–15*) were harvested from descending thoracic aortas obtained from the local abattoir by collagenase digestion; >98% of the resulting cells displayed uptake of acetylated low-density lipoprotein (Biomedical Technologies, Stoughton, MA). The cells were cultured in a humidified incubator (37°C, 5% CO_2) in growth medium consisting of Dulbecco's modified Eagle's medium (DMEM; GIBCO BRL, Gaithersburg, MD) supplemented with 10% calf serum (GIBCO BRL), 4 mM

0363-6143/97 $5.00 Copyright © 1997 the American Physiological Society

Downloaded from journals.physiology.org/journal/ajpcell at Tufts Univ (198.133.171.012) on November 15, 2026.

L-glutamine, 25 mM *N*-2-hydroxyethylpiperazine-*N*′-2-ethanesulfonic acid (pH 7.4), 10 U/ml of penicillin, and 10 μg/ml of streptomycin. Changes in cell viability were assessed by exclusion of propidium iodide uptake using a fluorescence-activated cell sorter (Becton Dickinson, Cockeysville, MD) and were found to be <5% under all conditions at the stimulus durations used.

To control cell shape, 10-cm petri dishes (model 8–757–13, Fisher Scientific, Pittsburgh, PA) with untreated nonadhesive surfaces were incubated at room temperature with solutions of RGD polymer (ProNectin F) at different concentrations (0, 0.01, 0.1, 0.5, and 2 μg/ml) for 30 min and then rinsed with phosphate-buffered saline (PBS) and allowed to dry overnight under ultraviolet irradiation for sterilization. BAEC suspensions (1×10^6 cells total, corresponding to a final density of 17×10^3 cells/cm^2) were then plated on each RGD-coated dish in DMEM containing 0.5 or 1% calf serum and allowed to spread for 18 h before analysis of cell shape and mRNA content.

In experiments addressing the role of cell seeding density, confluent monolayers of BAEC (3.25×10^6 cells) were trypsinized and triturated to maximize cell dissociation. The cell suspension was pelleted at low speed (200 *g*) and then resuspended in growth medium (containing 10% calf serum) and plated at serial dilutions from 1:16 (6.25% of initial density or 3.5×10^3 cells/cm^2) to 1:1 (100% of initial density or 55.5×10^3 cells/cm^2) on 10-cm tissue culture plates (model 3003, Falcon, Oxnard, CA) for 18 h prior to analysis.

To study the effect of serum content in the medium, confluent BAEC monolayers grown in 10-cm tissue culture plates were transferred to DMEM supplemented with increasing concentrations of serum (0, 1, 2.5, 5, and 10%) for 18 h before analysis.

RNA isolation and hybridization. The acid guanidium thiocyanate-phenol-chloroform method (22) was used to isolate total cellular RNA. Northern blot hybridization was performed with a random-primer ^{32}P-labeled 1.9-kilobase (kb) fragment of the bovine preproendothelin-1 cDNA (a kind gift of Dr. Thomas Quertermous), a 3.7-kb *Eco*R I fragment of the bovine constitutive endothelial nitric oxide synthase (eNOS; a kind gift of Dr. Thomas Michel), and a 1.3-kb *Pst*I fragment of the rat glyceraldehyde-3-phosphate dehydrogenase (GAPDH) cDNA. After incubation, the blots were serially washed in 2× saline sodium citrate (SSC)-1% sodium dodecyl sulfate (SDS) and 0.2× SSC-1% SDS to a final temperature of 55°C for ET-1 and at 63°C for GAPDH and then exposed to X-ray film (X-Omat-AR film, Kodak, Rochester, NY) at −80°C. Autoradiograms exposed in the linear range were subjected to two-dimensional densitometric scanning, and the signal strength of the band of interest was normalized for each sample with respect to the corresponding GAPDH mRNA signal.

Nuclear transcription runoff. Nuclei were isolated from BAEC that had been seeded for 18 h on either tissue culture plastic or petri dish surfaces coated with 0.01 μg/ml of ProNectin F and assayed using a previously described protocol (20, 22).

Peptide measurement. Medium supernatants were removed from BAEC plated on either tissue culture plastic or increasing concentrations of ProNectin F for 18 h and purified using Amprep Ethyl C2 columns from Amersham Life Science (Buckinghamshire, UK). ET-1 content was then measured in triplicate with a Biotrak enzyme-linked immunosorbent assay (ELISA) kit (Amersham Life Science), using the manufacturer's protocol.

Immunostaining. BAEC monolayers were washed three times with PBS, fixed with 3.7% paraformaldehyde in PBS for 30 min, permeabilized in PBS containing 0.1% Triton X-100 for 15 min and then washed in PBS. The fixed and permeabilized cells were then incubated with either monoclonal anti-phosphotyrosine antibody (clone 4G10, Upstate Biotechnology, Lake Placid, NY), or monoclonal anti-paxillin antibody (clone 349, Transduction Laboratories, Lexington, KY) for 30 min in PBS containing 1% bovine serum albumin (BSA), washed with PBS for 30 min and then incubated with anti-mouse Cy3-conjugated anti-mouse immunoglobulin G secondary antibody (Jackson Laboratories, West Grove, PA) for 30 min in PBS containing 1% BSA, washed with PBS for 30 min and fixed. For F-actin visualization, fixed and permeabilized cells were incubated with tetramethylrhodamine isothiocyanate (TRITC)-labeled phalloidin (Sigma) for 10 min, washed three times in PBS and then fixed with Mowiol (Calbiochem, San Diego, CA). Stained cells were visualized in an epifluorescence microscope (model BH-2, Olympus, Tokyo, Japan) and photographed with T-Max 400 film (Kodak).

Cell morphology analysis. Cells were visualized on an inverted microscope (Olympus model IMT-2) using phase-contrast or Hoffman phase-modulation optics and were photographed using T-Max 400 film (Kodak). Images were then scanned two-dimensionally to serve as input into the image and shape analysis program. Cell contour was traced manually, and connectivity analysis was performed on the resulting set of blobs using the Image Analyst software package (Automatix, Billerica, MA) on a Macintosh II/fx computer system (Apple, Cupertino, CA). The algorithm determined the best-fit ellipse through each cellular contour and provided the corresponding cell surface area value.

Statistics. Data are expressed as means ± SE. Statistical analysis was performed by analysis of variance and the unpaired Student's *t*-test.

RESULTS

CytD causes disruption of the F-actin cytoskeleton and induces cell rounding. Treatment of confluent endothelial monolayers with CytD resulted in retraction of cell edges followed by cell rounding (Fig. 1*A*, *left*). This phenomenon was a time-dependent process that was accelerated at higher CytD concentrations (data not shown). Staining with TRITC-phalloidin revealed complete dissolution of the fine F-actin microfilament network into a diffuse homogeneous staining pattern within the cell (Fig. 1*A*, *right*). Morphometric image analysis of the CytD-treated BAEC monolayers and computation of the projected cell area revealed a time-dependent decrease, from 570 ± 25 to 270 ± 24 μm^2/cell, which became statistically significant as early as 15 min after treatment (Fig. 1*B*).

CytD treatment induces decreased ET-1 mRNA expression in a time- and dose-dependent manner. Northern analysis performed on CytD-treated BAEC (0.2 μg/ml, 2 h) revealed a time-dependent decrease in ET-1 mRNA content that contrasted with unchanged GAPDH mRNA levels (Fig. 2*A*). The decrease in ET-1 mRNA was both time- and dose-dependent, with higher doses of CytD resulting in earlier and more pronounced downregulation of ET-1 mRNA levels (Fig. 2*B*).

Downloaded from journals.physiology.org/journal/ajpcell at Tufts Univ (198.133.171.012) on November 15, 2026.

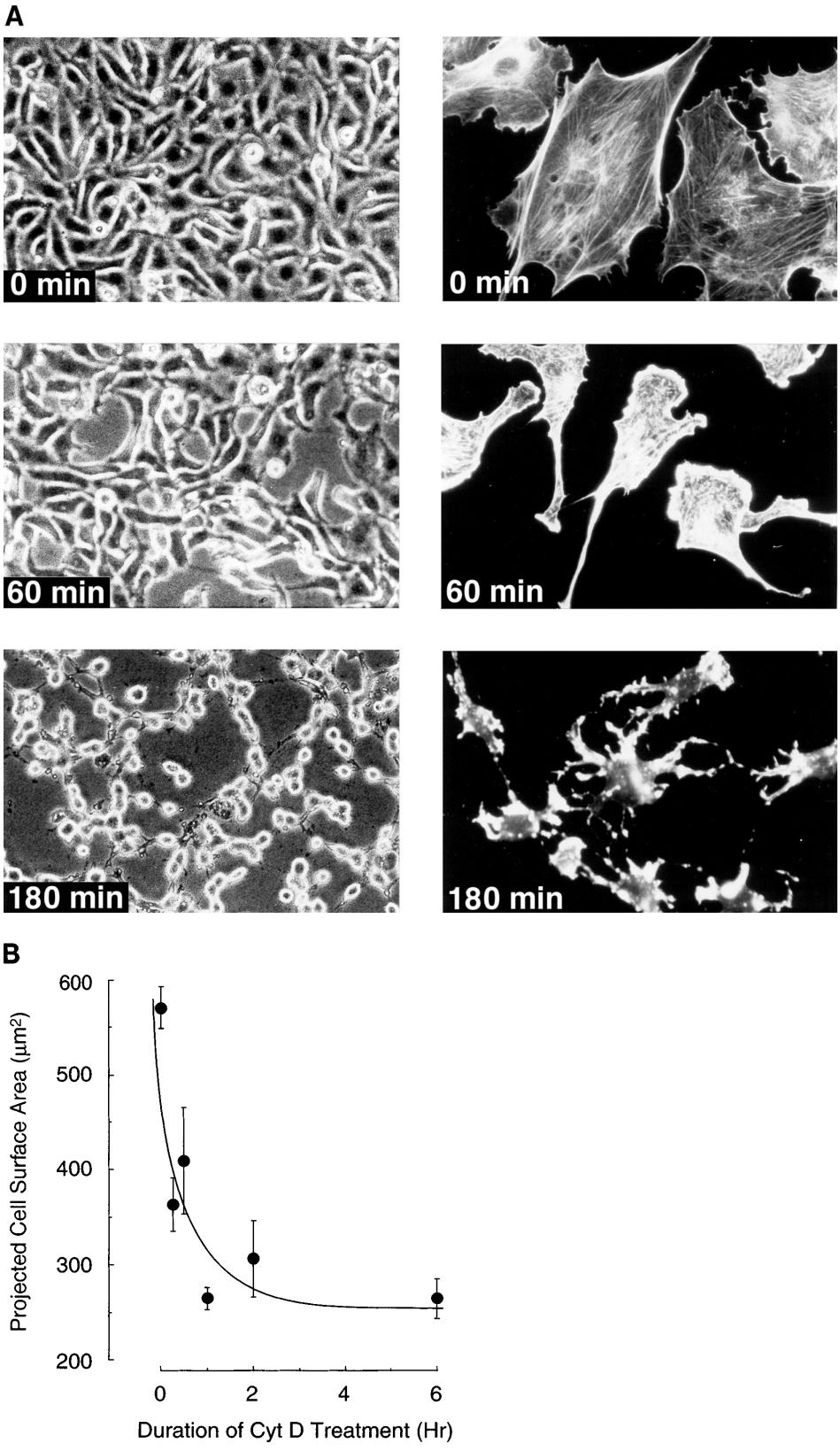


Fig. 1. Treatment of bovine aortic endothelial cells (BAEC) with cytochalasin D (CytD) results in cell process retraction and rounding. *A*: phase-contrast micrographs (*left*) of BAEC treated with CytD (0.2 μg/ml) for indicated times (0, 60, and 180 min) reveal retraction of cell processes and cell rounding. F-actin staining (*right*) with tetramethylrhodamine isothiocyanate (TRITC)-labeled phalloidin confirms rapid dissolution of F-actin fibers and cables with concomitant edge retraction and eventual rounding. *B*: quantitative morphometric analysis of projected cell surface area illustrates a 2- to 2.5-fold decrease in projected cell area in BAEC monolayers, occurring as soon as 15 min after onset of CytD addition.

Downloaded from journals.physiology.org/journal/ajpcell at Tufts Univ (198.133.171.012) on November 15, 2026.

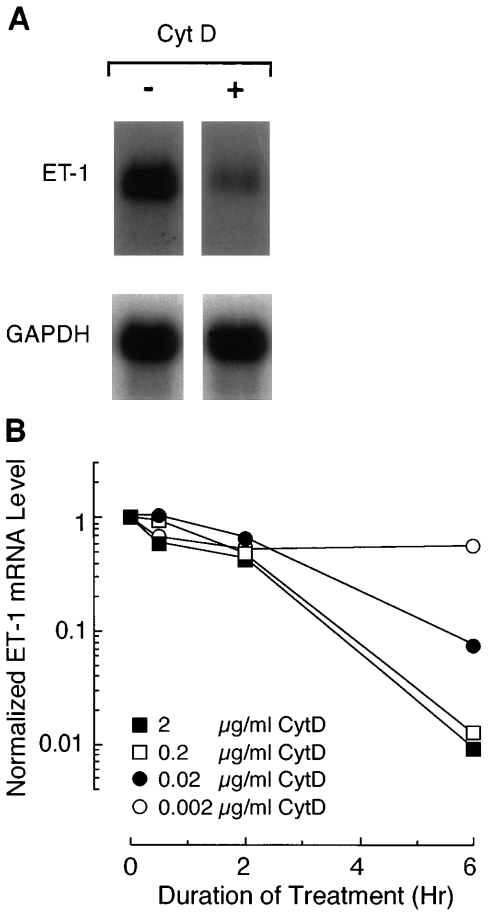


Fig. 2. CytD treatment induces a time- and dose-dependent downregulation of endothelin-1 (ET-1) mRNA expression. *A*: Northern blot analysis of BAEC monolayers treated with CytD (0.2 μg/ml) for 2 h shows a specific decrease in ET-1 mRNA content without significant change in glyceraldehyde-3-phosphate dehydrogenase (GAPDH). *B*: confluent monolayers of BAEC were treated with increasing concentrations of CytD (2×10^{-3} to 2 μg/ml) and harvested at 0, 0.5, 2, and 6 h for mRNA analysis. Densitometric analysis of ET-1 mRNA normalized with respect to GAPDH mRNA revealed a time- and dose-dependent decrease in ET-1 mRNA detectable within 0.5 h of treatment.

Forskolin, PMA, genistein and staurosporine induce changes in cell shape and F-actin network. To further test the link between endothelial shape, extent of cell spreading, and ET-1 mRNA content, we evaluated the effects of several pharmacological agents on the endothelial cytoskeleton. Forskolin and PMA both have been reported to induce BAEC retraction and cytoskeletal remodeling (Fig. 3*B*), with overall elongation, spindle formation, and significant decreases in projected cell surface area compared with control (Fig. 3*A*). PMA also induced dissolution of the coarse cable-like F-actin network (Fig. 3*F*) into a fine reticular staining pattern (Fig. 3*G*). Forskolin (10 μM) induced mild changes in cellular outline (Fig. 3*C*), subtle changes in actin staining pattern, and redistribution of F-actin stress fibers from the center to the periphery (Fig. 3*H*). Treatment with genistein (30 μM), a tyrosine kinase inhibitor, also caused cell process retraction, partial rounding (Fig. 3*D*), and moderate alteration of F-actin staining pattern with partial dissolution (Fig. 3*I*). Last, the protein kinase C (PKC) inhibitor staurosporine (10 nM) was also noted to induce BAEC rounding (Fig. 3*E*), which was nearly as dramatic as that induced by CytD (Fig. 3*I*), as well as time-dependent dissolution of actin filaments into a diffuse staining pattern (Fig. 3*J*). Thus four pharmacological agents acting through different second messenger systems, and (in the case of PMA and staurosporine) even having opposing stimulatory and inhibitory actions, each induced in parallel BAEC rounding and F-actin depolymerization.

Cell shape and F-actin changes induced by forskolin, PMA, genistein and staurosporine are accompanied by decreased expression of ET-1 mRNA. BAEC treated with forskolin (10 μM), PMA (100 nM), genistein (30 μM) and staurosporine (10 nM) were subjected to Northern analysis with ET-1 and GAPDH cDNA probes. Figure 4 shows that all four agents induced significant decreases in ET-1 mRNA within 6 h, without change in GAPDH mRNA level. This decrease in ET-1 mRNA level accompanied the endothelial cell shape retraction and F-actin staining loss in a manner similar to that observed with CytD treatment. This correlation among cell shape, the F-actin network, and ET-1 mRNA expression transcended any specific second messenger system, since the above agents individually acted via protein kinase A, PKC, tyrosine kinases, or directly via the microfilament network.

Steady-state endothelial cell shape and F-actin network can be controlled by varying RGD density on RGD polymer-coated nonadhesive petri dish surfaces. We next evaluated the relationship between cell shape and ET-1 mRNA level with an independent method for controlling steady-state cell shape. RGD polymer-coated petri dishes were seeded with BAEC, and cells were allowed to spread for 18 h. Figure 5 reveals that cells plated at a low RGD polymer concentration ([RGD]) assumed a round morphology (Fig. 5, *top left*) at steady state, whereas those plated at higher [RGD] appeared well spread and were indistinguishable from cells plated on standard tissue culture plastic (Fig. 5, *bottom right*).

The alteration of shape was also accompanied by changes in the endothelial microfilament network. The diffuse homogeneous staining in round cells plated at low [RGD] contrasted with the well-developed fibrillar F-actin network in spread cells plated at high [RGD] (Fig. 6), which was indistinguishable from that seen in cells plated on tissue culture plastic.

Variation of RGD polymer concentration reveals correlation between cell shape, F-actin network, and levels of ET-1 mRNA expression and secreted peptide. To test further the hypothesized link between cell shape, F-actin network, and ET-1 expression, we performed Northern analysis on BAEC cultured on RGD-coated nonadhesive petri dishes with variable RGD polymer plating density. Northern blot analysis (Fig. 7) and

Downloaded from journals.physiology.org/journal/ajpcell at Tufts Univ (198.133.171.012) on November 15, 2026.

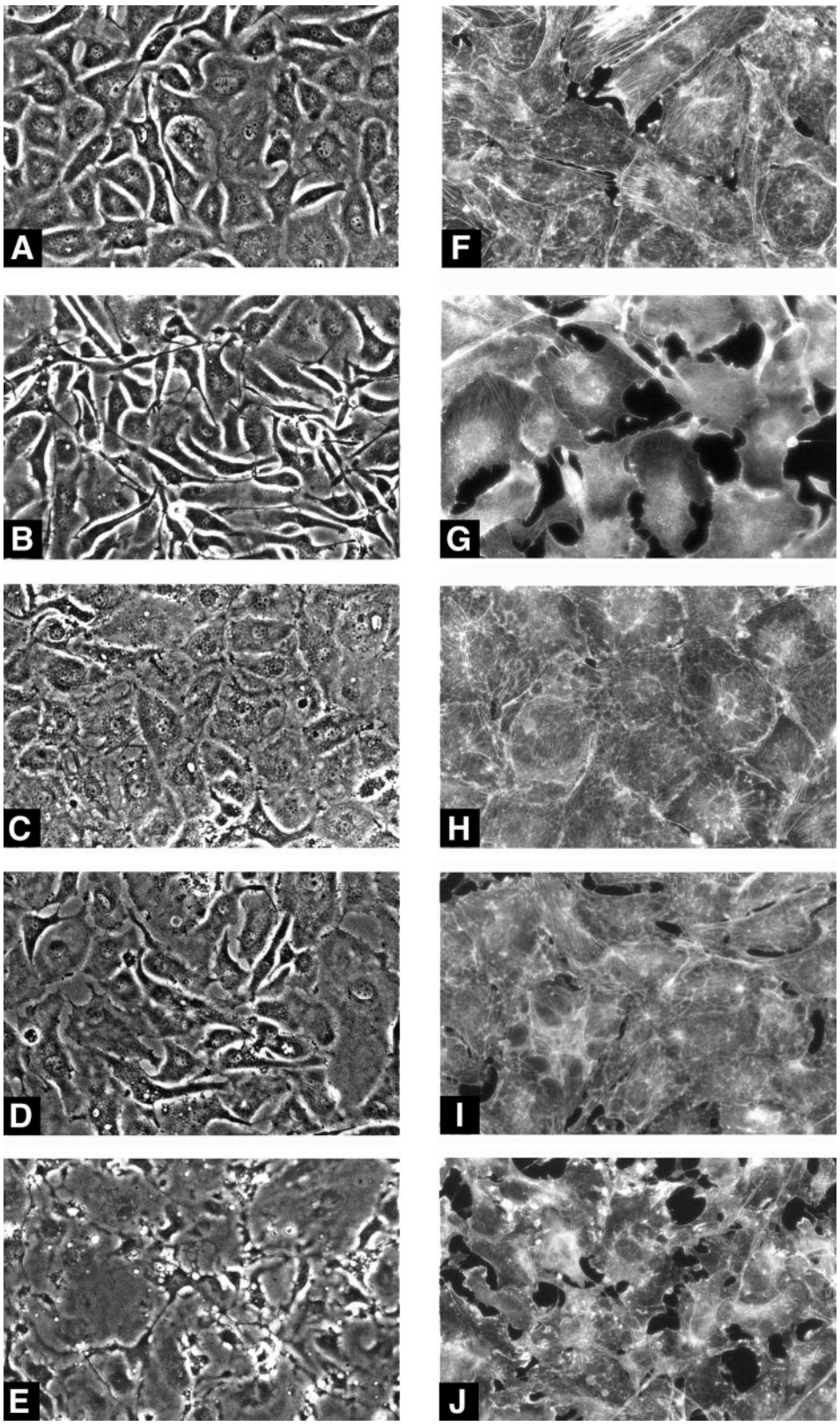


Fig. 3. Phorbol 12-myristate 13-acetate (PMA), forskolin, genistein, and staurosporine act on BAEC to induce cell shape change and F-actin dissolution. Phase-contrast micrographs (*A*–*E*) and F-actin staining (*F*–*J*) of confluent BAEC monolayers treated for 6 h with the protein kinase C (PKC) activator PMA (100 nM; *B* and *G*), the adenylate cyclase activator forskolin (10 μM; *C* and *H*), the tyrosine kinase inhibitor genistein (30 μM; *D* and *I*), and the PKC inhibitor staurosporine (10 nM; *E* and *J*), resulting in cell shape change including retraction and rounding compared with untreated controls (*A* and *F*). Actin staining with TRITC-phalloidin reveals significant remodeling and depolymerization of F-actin network to an extent that varies with agent used.

densitometry (Fig. 8) demonstrated low levels of ET-1 mRNA in round cells (low [RGD]) and high levels of ET-1 mRNA in spread cells (high [RGD]) that were indistinguishable from tissue culture plastic. The level of ET-1 mRNA normalized with respect to GAPDH decreased from 0.94 (arbitrary units) to 0.06, a 16-fold variation. In contrast, the level of constitutive eNOS mRNA was not significantly altered in the same cells,

Downloaded from journals.physiology.org/journal/ajpcell at Tufts Univ (198.133.171.012) on November 15, 2026.

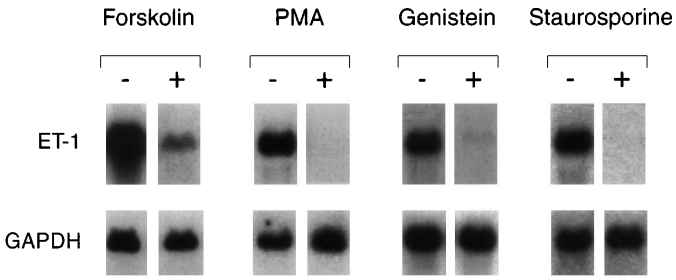


Fig. 4. Endothelial cell shape change and rounding observed in response to treatment with forskolin, PMA, genistein, and staurosporine are accompanied by downregulation of ET-1 mRNA. Confluent monolayers of BAEC were treated with forskolin (10 μM), PMA (100 nM), genistein (30 μM), or staurosporine (10 nM) and then harvested after 6 h for Northern analysis. Results show that all 4 treatments resulted in decreased ET-1 mRNA content without significant decrease in GAPDH mRNA, an effect that parallels cell rounding and cytoskeletal remodeling shown in Fig. 3.

with normalization to GAPDH mRNA levels showing a maximal variation of 15% across the entire range of [RGD] used. Quantitative morphometric analysis revealed an increase in projected cell surface area with increasing RGD polymer plating density (Fig. 8) from 91 to 412 μm^2. The clear correlation between BAEC shape, extent of spreading, and ET-1 mRNA content can be appreciated in Fig. 8. This correlation resembles that observed in the pharmacological manipulation experiments presented above (Fig. 4). The concentration of ET-1 peptide released into the supernatant was measured in BAEC spread on ProNectin F-coated petri dishes and quantitated using an ELISA kit. Although not as dramatic as the decrease in ET-1 mRNA, decreasing cell spreading resulted in an ~60% decrease in the amount of secreted ET-1 peptide when plating on 2 and 0.01 μg/ml ProNectin F were compared, indicating that the regulation is not limited to the RNA level but also extends to the final rate of peptide biosynthesis in and release from the endothelial cell (Fig. 9).

The decrease in ET-1 mRNA is the result of posttranscriptional control. To determine the mechanism of regulation of the ET-1 mRNA by cell shape control, nuclear runoff transcription assays were performed and revealed that cells in the round morphology demonstrated a higher (up to 80%) relative rate of ET-1 transcription when normalized with respect to GAPDH compared with cells in the spread morphology (Fig. 10). This finding points to a posttranscriptional mecha-

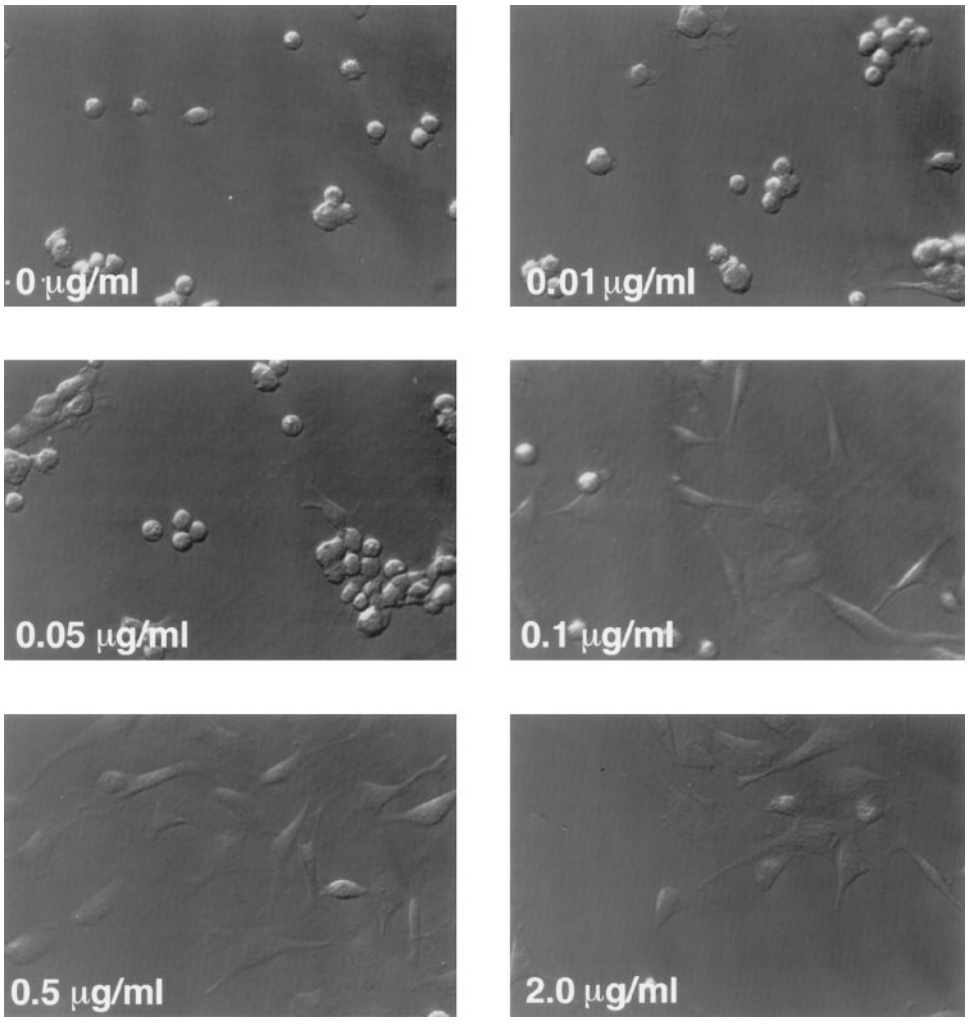


Fig. 5. Plating BAEC on various densities of synthetic RGD polymer on petri dishes controls cell shape and extent of cell spreading. Uncharged nonadhesive petri dish surfaces were preincubated with increasing concentrations of synthetic RGD polymer (ProNectin F; 0, 0.01, 0.05, 0.1, 0.5, and 2 μg/ml) and then rinsed with phosphate-buffered saline and allowed to air dry. Dispersed BAEC were then plated at a density of 17×10^3 cells/cm^2 on RGD-coated surfaces and allowed to spread for 18 h. Micrographs obtained using Hoffmann phase-modulation optics illustrate a dose-dependent increase of cell spreading with increasing RGD polymer density. Cells plated on surfaces treated with 2 μg/ml of RGD polymer (*bottom right*) were indistinguishable morphologically from those plated on standard tissue culture plastic.

Downloaded from journals.physiology.org/journal/ajpcell at Tufts Univ (198.133.171.012) on November 15, 2026.

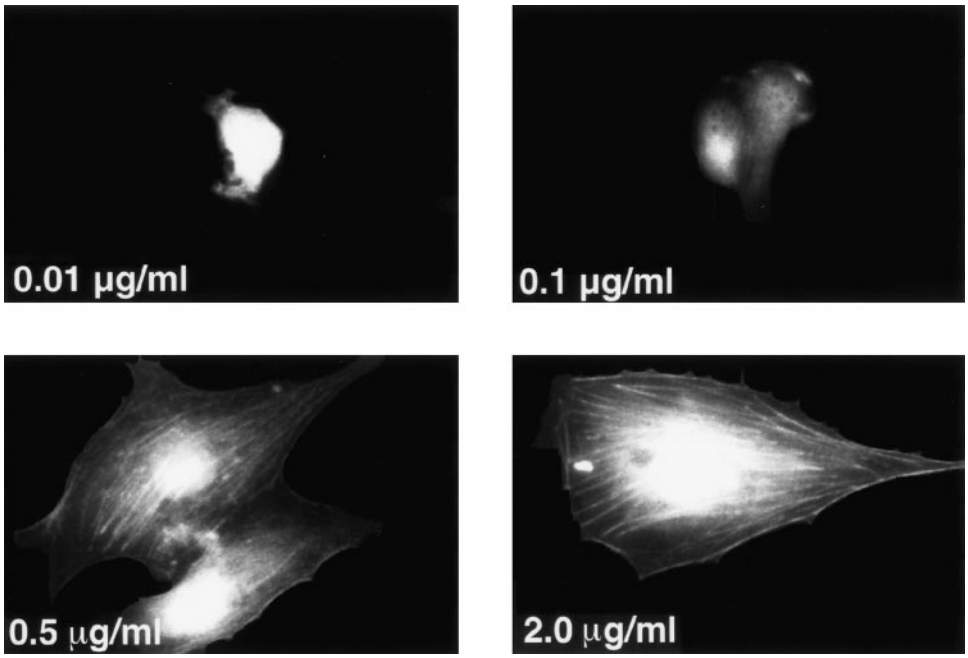


Fig. 6. Control of steady-state BAEC shape by RGD polymer correlates with state of F-actin network. Cells plated on various densities of synthetic RGD polymer on uncharged petri dishes were fixed after 18 h and stained with TRITC-phalloidin. Round cells plated on low RGD peptide density (0.01 and 0.1 μg/ml) revealed diffuse staining, whereas spread endothelial cells plated on higher densities (0.5 and 2 μg/ml) showed filamentous F-actin network.

nism, possibly that of mRNA destabilization, to explain the decreased level of ET-1 mRNA in round cells.

Extent of endothelial cell spreading is reflected in the physical distribution of paxillin and phosphotyrosine residues. To determine the potential role of focal adhesion contact-associated proteins in determining the relationship between BAEC shape and ET-1 gene expression, we analyzed the distribution of paxillin (Fig. 11), a focal adhesion contact-associated 70-kDa protein (3, 5) previously implicated in fibroblast adhesion and spreading on fibronectin (3). Increasing [RGD] resulted in increased cell spreading at steady state. This was accompanied by a change in the distribution of both paxillin and phosphotyrosine from a diffuse pattern to a punctate pattern with enhancement at the cell periphery.

Neither cell seeding density nor medium serum concentration can account for shape-dependent regulation of ET-1 gene expression. To evaluate the contribution of reduced cell density to the decreased ET-1 mRNA produced by cell rounding, secondary to CytD or to low [RGD], confluent monolayers of BAEC were trypsinized, triturated, replated in growth medium at cell seeding densities ranging from 6.25% (1:16 split corresponding to 3.5×10^3 cells/cm^2) to 100% (1:1 split or 55.5×10^3 cells/cm^2), and then harvested after 18 h. Quantitative Northern blot analysis revealed a decrease in ET-1 mRNA level at higher seeding density (Fig. 12*A*). Because cells plated at low [RGD] have fewer cell-cell contacts, increased ET-1 mRNA expression at lower seeding density suggests that the decreased ET-1 expression at lower [RGD] cannot be

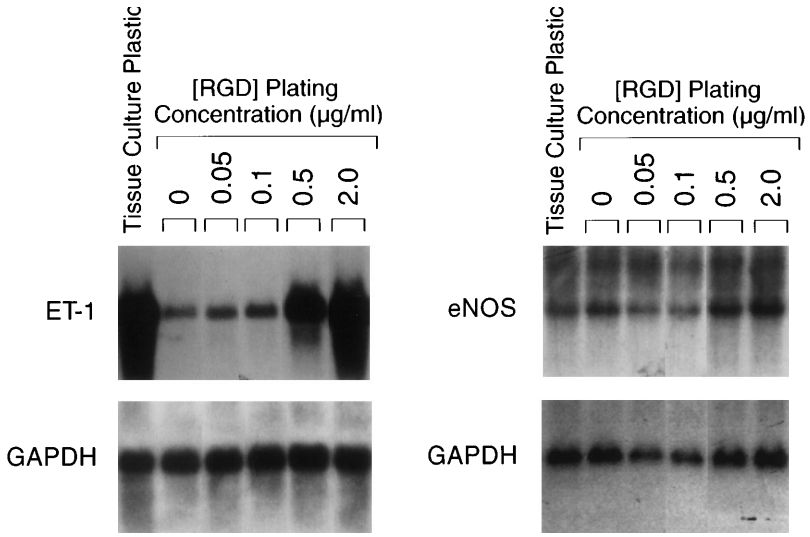


Fig. 7. Expression of ET-1 mRNA at steady state correlates closely with extent of cell spreading and indirectly with state of F-actin network, whereas endothelial nitric oxide synthase (eNOS) mRNA is independent. BAEC plated at 1:5 were allowed to spread on RGD-coated petri dishes or on tissue culture plastic for 18 h. *Left*: Northern blot analysis revealed low levels of ET-1 mRNA in round cells ([RGD] = 0, 0.05, and 0.1 μg/ml) and high levels in flattened cells ([RGD] = 0.5 and 2 μg/ml and tissue culture plastic). *Right*: in contrast, mRNA levels of eNOS were not significantly different between cells that were round, spread, or plated onto tissue culture plastic. GAPDH mRNA content was not altered as a function of cell shape change.

Downloaded from journals.physiology.org/journal/ajpcell at Tufts Univ (198.133.171.012) on November 15, 2026.

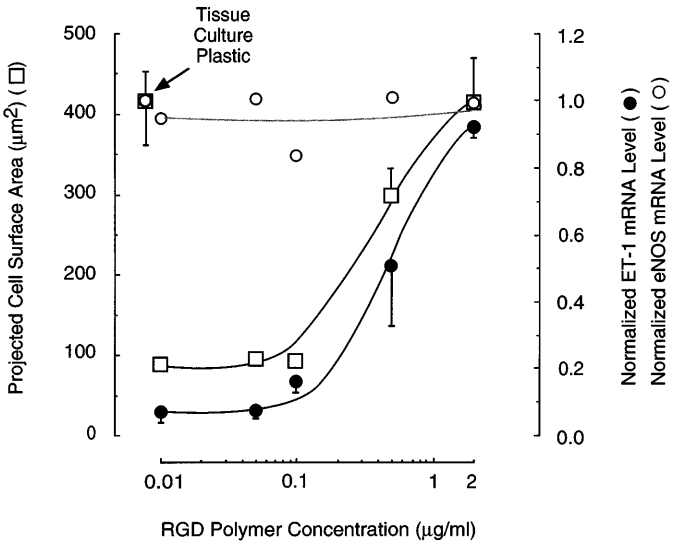


Fig. 8. Steady-state correlation of endothelial cell shape with expression of ET-1. Quantitative morphometric analysis (□) and ET-1 mRNA content normalized with respect to GAPDH (●) reveal concomitant increases in extent of spreading, as measured by projected cell area, and in normalized ET-1 mRNA content, as a function of [RGD]. In contrast, content of eNOS mRNA (○) did not change.

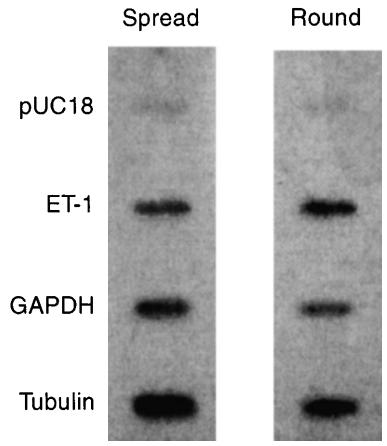


Fig. 10. Regulation of ET-1 mRNA level by cell shape control is not transcriptionally mediated. BAEC plated at 1:5 were allowed to spread in either well-spread morphology on tissue culture plastic or to remain in round morphology by plating on RGD-coated ([RGD] = 0.01 μg/ml) petri dishes for 18 h. Nuclei were then isolated and analyzed using a nuclear runoff transcription assay. Unlike mRNA level and peptide release, nuclear transcriptional rate is actually higher in round cells compared with spread cells with respect to not only GAPDH but also tubulin. pUC18, DNA vector hybridization specificity control.

accounted for on the basis of cell density or cell-cell contact.

Similarly, because cells plated on RGD polymer-coated plates were grown at low serum concentration (0.5–1%) to minimize the contribution of fibronectin in serum, we evaluated the effect of low serum concentration in the medium on specific ET-1 mRNA levels. Decreasing serum concentration increased ET-1 mRNA content by 1.4-fold (Fig. 12*B*). Thus decreased ET-1 expression at low [RGD] cannot be explained by decreased serum concentrations.

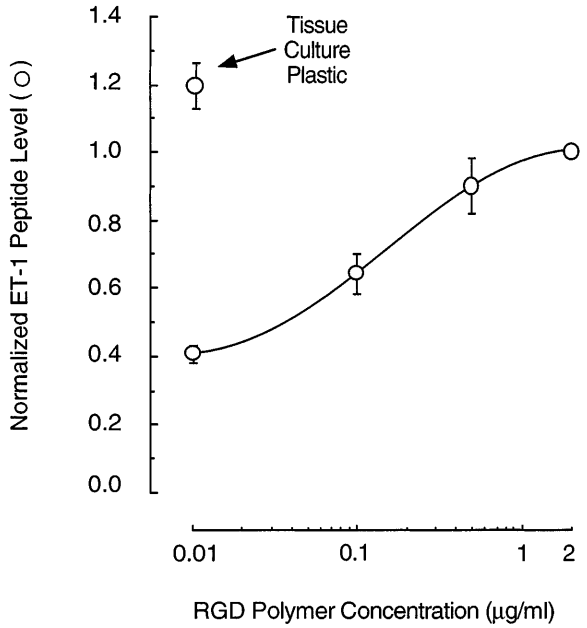


Fig. 9. Endothelial cell shape control affects release of ET-1 peptide. BAEC plated at 1:5 were allowed to spread on RGD-coated petri dishes or on tissue culture plastic for 18 h. Supernatant was then collected, purified, and quantitated, using an enzyme-linked immunosorbent assay kit for ET-1, and normalized with respect to value at [RGD] = 2 μg/ml. Amount of ET-1 peptide released into medium is significantly lower (by 60%) in round cells ([RGD] = 0.01 μg/ml) compared with flattened cells ([RGD] = 2 μg/ml).

DISCUSSION

This paper establishes a correlation between the abundance of ET-1 mRNA in BAEC, the state of the actin cytoskeleton, cell spreading, and cell shape. In particular, agents or maneuvers that depolymerize actin stress fibers and decrease cell spreading also decrease ET-1 mRNA levels. These effects occur in parallel not only in response to CytD, acting directly on the cytoskeleton, but also in response to perturbation of several distinct signaling pathways. These perturbations include activation of certain isoforms of PKC by PMA, activation of certain isoforms of adenylyl cyclase by forskolin, blockade of unidentified serine/threonine kinases by staurosporine, and blockade of unidentified tyrosine kinases by genistein. In addition, graded increases in cell rounding and decreases of cell spreading produced by plating cells onto various concentrations of RGD polymer were also accompanied by graded decreases in cell spreading, by depolymerization of the actin cytoskeleton, and by graded decreases in ET-1 mRNA content.

Thus the correlation between ET-1 mRNA abundance, cell spreading, cell shape, and the state of the actin cytoskeleton was maintained in a variety of growth conditions, both during acute treatments with soluble ligands and at nominally steady-state conditions 18 h after plating on substrata of RGD polymer. Several observations supported the specificity of this

Downloaded from journals.physiology.org/journal/ajpcell at Tufts Univ (198.133.171.012) on November 15, 2026.

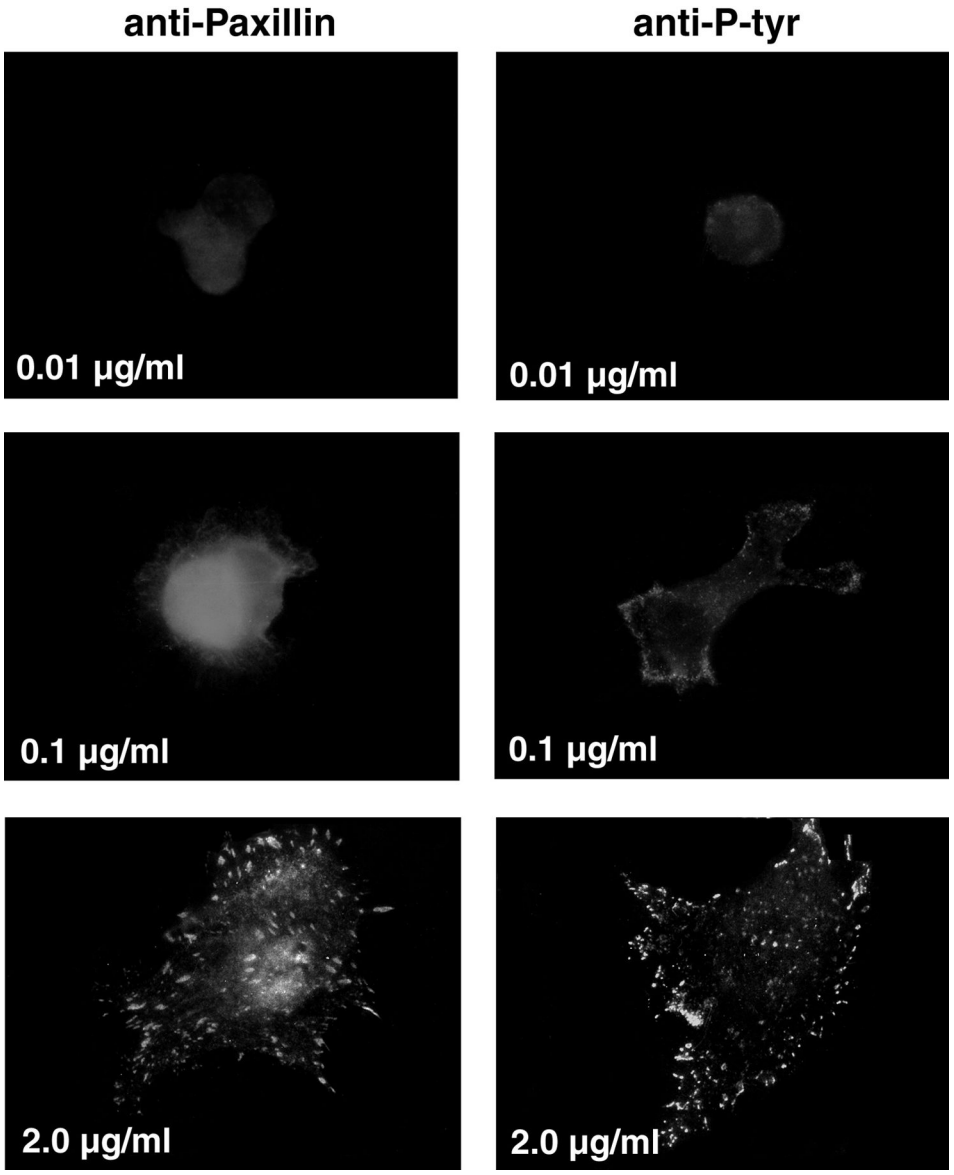


Fig. 11. Immunocytochemistry of paxillin and phosphotyrosine residues in BAEC plated at increasing [RGD]. BAEC plated at 1:5 were allowed to spread on RGD-coated petri dishes at [RGD] of 0.01 (*top*), 0.1 (*middle*) and 2 μg/ml (*bottom*) for 18 h and then stained with anti-paxillin antibody (*left*) or anti-phosphotyrosine antibody (anti-p-tyr; *right*). Note diffuse staining in round cells for both paxillin and tyrosine phosphorylation, which becomes progressively more punctate and localized to the cell periphery with increasing [RGD].

correlation with ET-1 mRNA. First, the level of mRNA of eNOS, an important enzyme involved in vasomotor control and previously shown to be upregulated by flow, was not affected by RGD-mediated cell shape control. Second, the correlation was not a primary consequence of changes in cell-cell contact, since decreased plating density increased, rather than decreased, ET-1 mRNA level. Third, the decreased serum concentrations in the RGD polymer experiments did not explain the decrease in ET-1 mRNA, since, in cells grown on tissue culture plastic, lowering serum concentration led to increased, rather than decreased, ET-1 mRNA. In addition, the regulation of ET-1 by cell shape was also found to extend to the peptide level, pointing to this control mechanism as being of functional significance in vasomotor control.

The mechanism by which the several examined stimuli downregulate ET-1 mRNA levels may be a reduction in the rate of ET-1 mRNA transcription or an increase in the rate of ET-1 mRNA degradation. Downregulation of ET-1 mRNA in BAEC secondary to application of laminar shear stress results in a reduction in the rate of transcription and has been mapped in the promoter of the ET-1 gene to a 5′ flanking region between ~2.5 and 2.9 kb upstream of the transcriptional initiation site (20). The nuclear run-on experiments performed in this study showed that cell rounding increased the rate of ET-1 transcription relative to both GAPDH and tubulin, suggesting posttranscriptional stability as the major mode of control in response to cell shape changes. ET-1 mRNA contains multiple AUUUA sequences and has previously been shown to increase in response to protein synthesis inhibitors such as cycloheximide (22). Whether this mechanism is shared with the one that regulates ET-1 mRNA transcription in response to the varied agents that depolymerize the actin cytoskeleton and cell shape modifiers remains to be determined.

Cell shape has previously been shown to affect phenotype and gene expression in other cell types. For

Downloaded from journals.physiology.org/journal/ajpcell at Tufts Univ (198.133.171.012) on November 15, 2026.

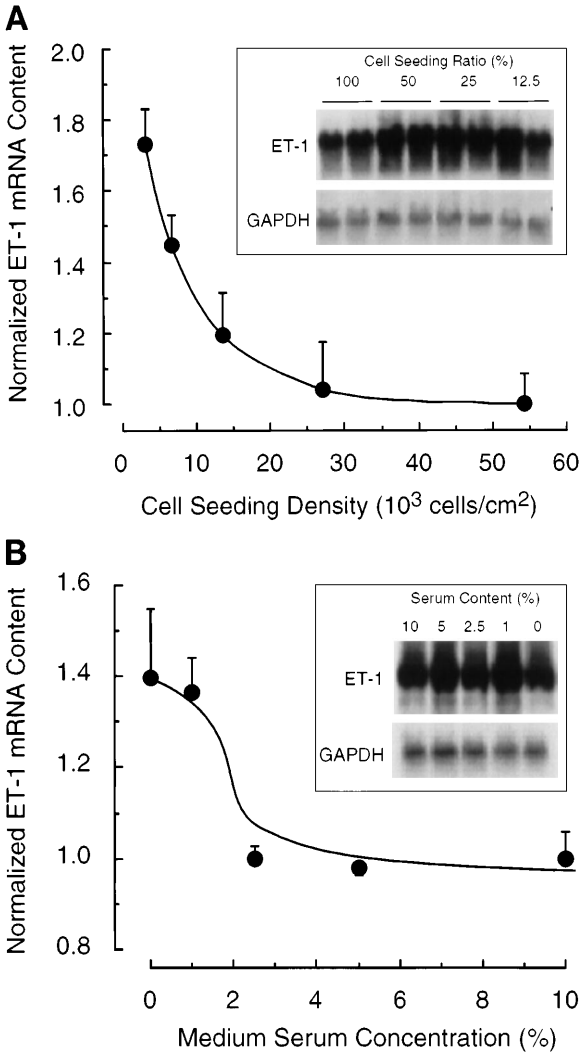


Fig. 12. Effect of endothelial cell density and serum concentration on expression of ET-1 gene. *A*: confluent monolayers of BAEC were trypsinized and replated at densities ranging from 3.5×10^3 cells/cm^2 (6.25% of confluent plate) to 55.5×10^3 cells/cm^2 (100%). After 18 h, total RNA was isolated and Northern blot analysis of ET-1 and GAPDH mRNA was performed (*inset*). Quantitative densitometric analysis of 3 independent experiments is shown. Note that cells plated at lowest density exhibited 1.7-fold higher levels of specific ET-1 mRNA content than did confluent monolayers. *B*: confluent BAEC were incubated for 18 h in presence of DMEM supplemented with 0, 1, 2.5, 5, or 10% serum. Total RNA was isolated and Northern blot analysis was performed (*inset*). Quantitative densitometry of 3 independent experiments revealed 1.4-fold higher ET-1 mRNA in presence of 0 or 1% serum than at higher concentrations.

instance, hepatocytes (2, 25) and mammary gland cells (19) plated on substrata that allow attachment and round cell morphology maintain tissue-specific gene expression and an anabolic phenotype in the absence of cell proliferation. When these cells are grown on a surface that allows spreading, they dedifferentiate and enter the cell cycle. Recently, Hansen et al. (12) have shown that cell spreading promotes and accelerates passage through the G_1-S transition of the cell cycle and shuts off the intrinsic hepatocyte differentiation program.

Though numerous signal transduction pathways appear to link the state of the actin cytoskeleton to the abundance of ET-1 mRNA in BAEC, the identity of the downstream steps remains unknown, as does the possible existence of a downstream signal integrator. However, the results of Kolodney and Wysolmerski linking endothelium-generated isometric force to the state of the actin network (18) suggest intracellular tension, transmitted throughout the microfilament network and acting at focal adhesion contacts, as a possible candidate (5, 15). Recent work has revealed clustering at focal adhesion complexes of growth factor receptors, signaling molecules such as pp60$^{c\text{-}src}$, phosphatidylinositol-3-kinase, phospholipase C, and the Na^+/H^+ antiporter, and actin cytoskeleton binding proteins such as talin, vinculin, paxillin, and α-actinin. These findings, in conjunction with data of Wang et al. (37) showing that externally applied stresses can be transmitted via focal adhesion contacts through the cytoskeleton, have led to the proposal of a tensegrity-based model (7, 15). In this model, externally applied stresses or cell shape change are translated into altered intracellular tension, which is borne by the microfilament network and is transmitted to focal adhesion contacts. There, intracellular tension may alter the conformation or activity of one or more focal adhesion contact-associated signaling molecules with subsequent downstream effects on gene expression and cellular phenotype via a yet undefined signaling system.

Consistent with the intracellular tension hypothesis, we have observed that lysophosphatidic acid, which activates Rho, a Ras-related GTP-binding protein known to stimulate stress fiber induction, focal adhesion formation, increased tyrosine phosphorylation (30), and intracellular tension (4), induced actin stress fibers in confluent BAEC and increased specific ET-1 mRNA content by twofold. In contrast, compound H-7, a broad-range protein kinase inhibitor that inhibits actomyosin contractility independently from its action on PKC (36) and that has been shown to decrease stress fibers, focal adhesion formation, and tyrosine phosphorylation (4), specifically decreased ET-1 mRNA levels. Also consistent with this hypothesis, the recently discovered natural cyclic peptide jasplakinolide, which binds to F-actin at the phalloidin site (31), induced cell rounding, stress fiber dissolution, and ET-1 mRNA decrease (unpublished data). The altered distribution of paxillin and phosphotyrosine residues with cell shape spreading at steady state (Fig. 11) provides a potential link between cell shape and the signaling systems that may lead to downstream altered ET-1 gene expression.

In conclusion, we have shown that cell shape and the state of the microfilament network are potent regulators of ET-1 expression and have presented data suggesting that this regulation may be mediated by intracellular tension through posttranscriptional processing. Further work will be required to identify the molecular links and mechanisms by which intracellular tension may control gene regulation.

This work was supported by a Whitaker Foundation Grant, a Johnson & Johnson Foundation Research Grant (through the Harvard-Massachusetts Institute of Technology Health Sciences and Technology Division), National Institutes of Health Grants P30-HL-

Downloaded from journals.physiology.org/journal/ajpcell at Tufts Univ (198.133.171.012) on November 15, 2026.

15157 (through the Boston Sickle Cell Center) and P60-DK-34854 (through the Harvard Digestive Diseases Center), and a National Institutes of Health Medical Scientist Training Program stipend to A. Malek.

S. Izumo and S. L. Alper are Established Investigators of the American Heart Association.

Current address of A. M. Malek: Neurointerventional Radiology, University of California, San Francisco, Box 0628, L352, 505 Parnassus Ave., San Francisco, CA 94143.

Address for reprint requests: S. Izumo, Rm. SL-201, or S. L. Alper, Rm. RW-763, Beth Israel Deaconess Medical Ctr., East Campus, 330 Brookline Ave., Boston, MA 02215.

Received 3 January 1997; accepted in final form 16 July 1997.

REFERENCES

1. **Adams, D. S.** Mechanisms of cell shape change: the cytomechanics of cellular response to chemical environment and mechanical loading. *J. Cell Biol*. 117: 83–93, 1992.
2. **Ben-Ze'ev, A., G. S. Robinson, and R. Farmer.** Cell-cell and cell-matrix interactions differentially regulate the expression of hepatic and cytoskeletal genes in primary cultures of rat hepatocytes. *Proc. Natl. Acad. Sci. USA* 85: 2161–2165, 1988.
3. **Burridge, K., C. E. Turner, and E. Romer.** Tyrosine phosphorylation of paxillin and pp125FAK accompanies cell adhesion to extracellular matrix: a role in cytoskeletal assembly. *J. Cell Biol*. 119: 893–903, 1992.
4. **Chrzanowska-Wodnicka, M., and K. Burridge.** Rho-stimulated contractility drives the formation of stress fibers and focal adhesions. *J. Cell Biol*. 133: 1403–1415, 1996.
5. **Clark, E. A., and J. S. Brugge.** Integrins and signal transduction pathways: the road taken. *Science* 268: 233–239, 1995.
6. **Davies, P. F.** Flow-mediated endothelial mechanotransduction. *Physiol. Rev*. 75: 519–560, 1995.
7. **Dennerl, T. J., H. C. Joshi, L. E. Steel, R. E. Buxbaum, and S. R. Heidemann.** Tension and compression in the cytoskeletal structure of PC-12 neurites. II. Quantitative measurements. *J. Cell Biol*. 107: 655–674, 1988.
8. **DePaola, N., M. J. Gimbrone, P. F. Davies, and C. J. Dewey.** Vascular endothelium responds to fluid shear stress gradients. *Arterioscler. Thromb*. 12: 1254–1257, 1992.
9. **Franke, R., M. Gräfe, H. Schnittler, D. Seiifge, C. Mittermayer, and D. Drenckhahn.** Induction of human vascular endothelial stress fibers by fluid shear stress. *Nature* 307: 648–649, 1984.
10. **Girard, P. R., and R. Nerem.** Shear stress modulates endothelial cell morphology and F-actin reorganization through the regulation of focal adhesion-associated proteins. *J. Cell. Physiol*. 163: 179–193, 1995.
11. **Goode, T., P. F. Davies, M. A. Reidy, and D. E. Bowyer.** Aortic endothelial cell morphology observed in situ by scanning electron microscopy during atherogenesis in the rabbit. *Atherosclerosis* 27: 235–251, 1977.
12. **Hansen, L. K., D. J. Mooney, J. P. Vacanti, and D. E. Ingber.** Integrin binding and cell spreading on extracellular matrix act at different points in the cell cycle to promote hepatocyte growth. *Mol. Cell. Biol*. 5: 967–975, 1994.
13. **Harris, A. K., P. Wild, and D. Stopak.** Silicon rubber substrate: a new wrinkle in the study of cell locomotion. *Science* 208: 177–179, 1980.
14. **Herman, I. M., A. M. Brant, V. S. Warty, J. Bonaccorso, E. C. Klein, R. L. Kromos, and H. S. Borovetz.** Hemodynamics and the vascular endothelial cytoskeleton. *J. Cell Biol*. 105: 291–302, 1987.
15. **Ingber, D.** Cellular tensegrity: defining new rules of biological design that govern the cytoskeleton. *J. Cell Sci*. 104: 613–627, 1993.
16. **Ingber, D. E., D. Prusty, J. V. Frangioni, E. J. Cragoe, C. Lechene, and M. A. Schwartz.** Control of intracellular pH and growth by fibronectin in capillary endothelial cells. *J. Cell Biol*. 110: 1803–1811, 1990.
17. **Kim, D. W., A. I. Gottlieb, and B. L. Langille.** In vivo modulation of endothelial F-actin microfilaments by experimental alterations in shear stress. *Arteriosclerosis* 9: 439–445, 1989.
18. **Kolodney, M. S., and R. B. Wysolmerski.** Isometric contraction by fibroblasts and endothelial cells in tissue culture: a quantitative study. *J. Cell Biol*. 117: 73–82, 1992.
19. **Li, M. J., J. Aggeler, D. A. Farson, C. Hatier, J. Hassell, and M. F. Bissell.** Influence of a reconstituted basement membrane and its components on casein gene expression and secretion in mouse mammary epithelial cells. *Proc. Natl. Acad. Sci. USA* 84: 136–140, 1987.
20. **Malek, A. M., A. L. Greene, and S. Izumo.** Regulation of endothelin-1 gene by fluid shear stress is transcriptionally mediated and independent of protein kinase C and cAMP. *Proc. Natl. Acad. Sci. USA* 90: 5999–6003, 1993.
21. **Malek, A. M., and S. Izumo.** Control of endothelial cell gene expression by flow. *J. Biomech*. 28: 1515–1528, 1995.
22. **Malek, A. M., and S. Izumo.** Mechanism of endothelial cell shape change and cytoskeletal remodeling in response to fluid shear stress. *J. Cell Sci*. 109: 713–726, 1996.
23. **Malek, A. M., and S. Izumo.** Molecular aspects of signal transduction of shear stress in the endothelial cell. *J. Hypertens*. 12: 989–999, 1994.
24. **Masuda, H., N. Saito, K. Kawamura, M. Sageshima, T. Shozawa, and A. Kanazawa.** Flow loaded canine carotid artery. I. A morphometric study of microfilament bundles in endothelial cells. *Acta Pathol. Jpn*. 36: 1833–1842, 1986.
25. **Mooney, D., L. Hansen, J. Vacanti, R. Langer, S. Farmer, and D. Ingber.** Switching from differentiation to growth in hepatocytes: control by extracellular matrix. *J. Cell. Physiol*. 151: 497–505, 1992.
26. **Morel, N. M. L., P. P. Petruzzo, H. B. Hechtman, and D. Shepro.** Pulmonary microvascular endothelial cell contractility on silicone rubber substrate. *J. Cell. Physiol*. 141: 653–659, 1989.
27. **Nerem, R. M., M. J. Levesque, and J. F. Cornhill.** Vascular endothelial morphology as an indicator of the pattern of blood flow. *J. Biomech. Eng*. 103: 172–177, 1981.
28. **Prasad, A. R., S. A. Logan, R. M. Nerem, C. J. Schwartz, and E. A. Sprague.** Flow-related responses of intracellular inositol phosphate levels in cultured aortic endothelial cells. *Circ. Res*. 72: 827–836, 1993.
29. **Remuzzi, A., C. F. Dewey, Jr., P. F. Davies, and M. A. Gimbrone, Jr.** Orientation of endothelial cells in shear fields in vitro. *Biorheology* 21: 617–630, 1984.
30. **Ridley, A. J., and A. Hall.** The small GTP-binding protein rho regulates the assembly of focal adhesions and actin stress fibers in response to growth factors. *Cell* 70: 389–399, 1992.
31. **Rubb, M. R., A. M. J. Senderowicz, E. A. Sausville, K. L. K. Duncan, and E. Korn.** Jasplakinolide, a cytotoxic natural product, induces actin polymerization and competitively inhibits the binding of phalloidin to F-actin. *J. Biol. Chem*. 269: 14869–14871, 1994.
32. **Sakai, S., T. Miyauchi, M. Kobayashi, I. Yamaguchi, K. Goto, and Y. Sugishita.** Inhibition of myocardial endothelin pathway improves long-term survival in heart failure. *Nature* 384: 353–355, 1996.
33. **Shirinsky, V. P., A. S. Antonov, K. G. Birukov, A. V. Sobolevsky, Y. A. Romanov, N. V. Kabaeva, G. N. Antonova, and V. N. Smirnov.** Mechano-chemical control of human endothelium orientation and size. *J. Cell Biol*. 109: 331–339, 1989.
34. **Sumpio, B. E., A. J. Banes, M. Buckley, and G. J. Johnson.** Alterations in aortic endothelial cell morphology and cytoskeletal protein synthesis during cyclic tensional deformation. *J. Vasc. Surg*. 7: 130–138, 1988.
35. **Tamirisa, P., W. H. Frishman, and A. Kumar.** Endothelin and endothelin antagonism: roles in cardiovascular health and disease. *Am. Heart J*. 130: 601–610, 1995.
36. **Volberg, T., B. Geiger, S. Citi, and A. D. Bershadsky.** Effect of protein kinase inhibitor H7 on the contractility, integrity, and membrane anchorage of the microfilament system. *Cell Motil. Cytoskeleton* 29: 321–338, 1994.
37. **Wang, N., J. P. Butler, and D. E. Ingber.** Mechanotransduction across the cell surface and through the cytoskeleton. *Science* 260: 1124–1127, 1993.
38. **Ziegelstein, R. C., L. Cheng, and M. C. Capogrossi.** Flow-dependent cytosolic acidification of vascular endothelial cells. *Science* 258: 656–659, 1992.

Downloaded from journals.physiology.org/journal/ajpcell at Tufts Univ (198.133.171.012) on November 15, 2026.